

Diamond kinoform hard X-ray refractive lenses: design, nanofabrication and testing

A. F. Isakovic,^{a*} A. Stein,^b J. B. Warren,^{b,c} S. Narayanan,^d M. Sprung,^d A. R. Sandy^d and K. Evans-Lutterodt^a

^aBrookhaven National Laboratory, NSLS, Upton, NY, USA, ^bBrookhaven National Laboratory, CFN, Upton, NY, USA, ^cBrookhaven National Laboratory, Instrumentation Division, Upton, NY, USA, and ^dArgonne National Laboratory, Argonne, IL, USA. E-mail: isakovic@bnl.gov

Motivated by the anticipated advantageous performance of diamond kinoform refractive lenses for synchrotron X-ray radiation studies, this report focuses on progress in designing, nanofabricating and testing of their focusing performance. The method involves using lift-off and plasma etching to reproduce a planar definition of numerically determined kinoform refractive optics. Tests of the focusing action of a diamond kinoform refractive lens at the APS 8-ID-I beamline demonstrate angular control of the focal spot.

Keywords: focusing hard X-rays; kinoform refractive optics; diamond; silicon; etching.

1. Introduction and motivation

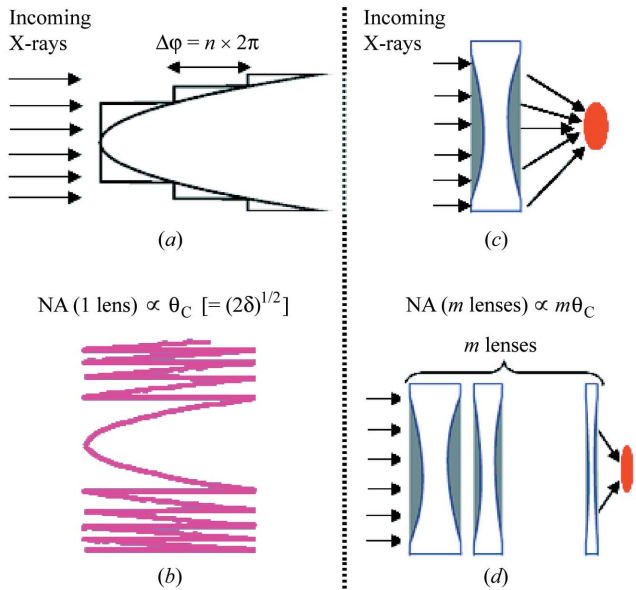
The exceptional properties of diamond have assured its use in a wide range of applications despite its cost and the difficulties in working with it. Nöhammer *et al.* (2003) realised quite early that diamond offered several distinct advantages as an optic material for producing hard X-ray ($E > 4$ keV) refractive lenses, including its relatively large decrement in refractive index, relatively low absorption and high thermal conductivity. The thermal properties of diamond are likely to be explored for the nanofabrication of X-ray focusing refractive optics with the ability to withstand the high heat loads at future synchrotron sources (NSLS-II, for example). Unfortunately, making such high-quality focusing optics requires precision ‘sculpting’ of the lens material to minimize phase errors in the final optics, which is difficult to achieve in diamond. Consequently, many hard X-ray optics have been fabricated from silicon that, while not the ideal material, is much easier to shape in accordance with a numerically predetermined shape. Here, the procedures are described that were used to fashion a satisfactory kinoform lens from diamond.

A variety of research approaches have been taken to improve the quality of hard X-ray optics, emphasizing the need for high spatial resolution. The existing creative proposals and ongoing research programs for nanometer-scale focused hard X-ray beams fall broadly into groups with the three familiar diffractive, reflective and refractive limits. Those with diffractive limits include multilayer Laue lenses (Kang *et al.*, 2006, and references therein) and the more traditional Fresnel zone plates (Chao *et al.*, 2005, and references therein; Schroer, 2006), including commercially available zone plates (<http://xradia.com/>). The reflective limit encompasses traditional solid-metal mirrors (Rau *et al.*, 2006; Yumoto *et al.*, 2006; Mimura *et al.*, 2007), capillaries (Bilderback *et al.*, 1994;

Snigirev *et al.*, 2007) and the non-traditional multilayer mirror (Rau *et al.*, 2006). The refractive limit covers, for example, compound refractive lenses (Suehiro *et al.*, 1991; Lengeler *et al.*, 1998, and references therein) and the less traditional kinoform optics (Aristov *et al.*, 2000; Cremer *et al.*, 1999; Evans-Lutterodt *et al.*, 2007; Nazmov *et al.*, 2004, and references therein). Several other approaches to attain the required improvements are being considered, most notably the clessidra lens array (Jark *et al.*, 2008; De Caro & Jark, 2008), tapered waveguides (Bergemann *et al.*, 2003) and the sawtooth-like lens (Shastri *et al.*, 2007). In this article the kinoform optic is considered: it is demonstrated that implementing such an optic with diamond material can yield a high-resolution optic with high transmissivity.

Kinoforms (Jordan *et al.*, 1970) are computer-generated phase optics that, upon illumination, deliver an image of the mathematically desired object. The optimal phase-profile for a kinoform is calculated using Fermat’s theorem (Moreno *et al.*, 1997; Hudson, 1984; Goodman, 1986) on path lengths, together with a knowledge of the phase properties of the incident illumination and the desired final object. For example, lens kinoforms can be formed wherein the desired object is a single point, and the incident illumination is a parallel plane wave. A key feature of ideal kinoforms is that they can yield efficiencies of 100% in the image (Sweatt, 1977; Erko *et al.*, 1996). The inset of Fig. 1(a) is a schematic of a conventional ‘long’ kinoform design, showing the curved interior profile derived from the solid refractive optic, and the discontinuous exterior profile after removing sections so resulting in improved transmission relative to the solid refractive optic. Given a refractive index

$$n = 1 - \delta + i\beta, \quad (1)$$


Figure 1

(a) An example of a conventional kinoform lens design, also called a ‘long kinoform’. (b) An example of a ‘short kinoform’ lens that is more practical for compound lenses made *via* the planar nanofabrication approach. (c) and (d) Schematic demonstration of modifying the numerical aperture (and of the resolution) in a compound lens set-up. Design and nanofabrication ensure that each kinoform lens in a compound kinoform optics is slightly different from the preceding one.

parallel illumination and a point focus at a focal length F , the profile for a solid refractive loss-less lens is

$$y^2 + (2\delta - \delta^2)x^2 - 2\delta Fx = 0, \quad (2)$$

i.e. an ellipse. The kinoform profile is obtained by simply removing material of size integer multiples of λ/δ , where λ is the desired operating wavelength. The segments of size $N\lambda/\delta$ correspond to multiples of the 2π phase shift at the design wavelength λ ; thus, the optic behaves like the corresponding solid refractive optic, but its transmission is better. For completeness, Fig. 1(b) depicts the ‘short’ kinoform that is derived from the ‘long’ kinoform by folding all the segments back into a single plane, while keeping the entire profile compatible with the Fermat theorem. The ‘long’ and ‘short’ kinoforms emphasize two equivalent ways of attaining the ideal kinoform at the design energy, either as a perfectly blazed zone plate or an array of perfectly coherent micro-lenses.

For structures of this type, the transmission is asymptotically

$$t = \exp(-2\pi N\beta/\delta) \quad (3)$$

for features that are $N\lambda/\delta$ in size, corresponding to $2N\pi$ phase shifts. As Evans-Lutterodt *et al.* (2004) pointed out, a kinoform design often incorporates features larger than the minimum λ/δ to ease manufacturing of the optics; however, the transmission of the optic suffers accordingly. To maximize transmission through these optics, materials with β/δ as small as possible must be chosen.

A second reason to consider carefully the materials for these optics is that achieving high spatial resolution requires employing compound kinoforms, as sketched in Fig. 1(d), rather than a single lens, sketched in Fig. 1(c). A single lens for the parallel-to-point configuration entails having an elliptical cross section, thereby setting the resolution for a single lens at no better than $0.61\lambda/\theta_C$, where $\theta_C = (2\delta)^{1/2}$ is the critical angle. Lens arrays can be designed in which each successive lens is optimized using Fermat’s theorem to focus the wavefield from the previous lens, so exceeding the critical angle limit (Evans-Lutterodt *et al.*, 2007), but this configuration reduces transmission. If t is the transmission of a single lens, one can show that the gain of an array of M lenses is Mt^M , and the optimal gain is obtained for $\ln(1/t) \simeq 1/M$. However, if concern is less about the gain in the focal spot and more about the resolution, then one simply can have as many lenses as is required to achieve the desired resolution, but with less than the optimal transmission of t^M . In such a case, each of the half-shells is numerically calculated (shaped) and positioned (as a parallel side feature) using Fermat’s theorem so that the entire body of the backfolded lens has one focal spot.

A final consideration about the lens material is that it should be single-crystal material or perfectly amorphous because hard X-ray photons are sensitive to material imperfections, such as grain boundaries; since such faults scatter light in the forward direction, they form a background to the focused spot and thus decrease the signal-to-noise ratio (Ognev, 2005). To date, silicon has been the most common material used in fabricating these lenses. However, the above considerations clearly imply that a material with better transmission than silicon will exhibit improved optic performance. At a photon wavelength of 0.1 nm corresponding to 12.39 keV, the attenuation length of silicon is 0.25 mm while that of diamond is 3.9 mm, a 16-fold improvement; undoubtedly, diamond will be a superior material for making the lenses (NIST database: <http://physics.nist.gov/PhysRefData/>). To quantify and verify this conclusion, a comparison is needed of the transmission of silicon and diamond lenses as a function of energy, and M , the number of lenses. For the hard X-ray range of energies of primary concern to the synchrotron community (*i.e.* 4 keV < E < 200 keV), the elastic cross section falls as $\sim E^{-2}$, and the primary mechanisms for X-ray attenuation are the photoelectric and the Compton scattering cross sections. While the photoelectric cross section falls as $\sim E^{-3}$, the Compton cross section rises with increasing photon energy; the combination of these three terms results in a cross-over behavior illustrated for diamond in Fig. 2(a) and for silicon in Fig. 2(b). For a single diamond lens (circles) there is a maximum transmission of 99.6% at the photon energy of 18.8 keV. Two more observations follow from the analysis in Fig. 2. If the same transmissivity is required for both materials, there is a demonstrable shift in the energy range towards higher energies for silicon lenses that becomes progressively worse (*i.e.* increasingly outside the normal operating range of many contemporary synchrotron beamlines) with an increasing number of lenses. Accordingly, silicon-based compound kinoform refractive lenses are at a disadvantage

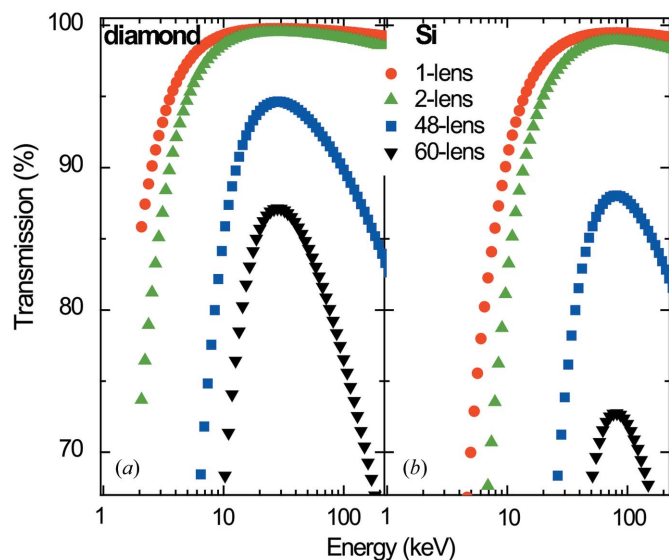


Figure 2
 Calculated transmissivity of (a) diamond-based kinoform refractive lenses and (b) silicon-based kinoform refractive lenses, in a broad hard X-ray range. Symbols for the number of lenses are common to both panels.

when faced with the task of obtaining a better resolution and numerical aperture.

The reasons that diamond lenses are not as widespread as might be anticipated largely reflect a lack of high-quality repeatable nanofabrication methods and the availability of affordable single-crystal diamonds. This report addresses the first of the two obstacles, while working with a lower quality polycrystalline diamond. The basic justification is that the following major corrections anticipated from transferring this process to a single-crystal diamond will be attainable: a change in the etch rate, and a re-distribution of the heat load, with the net change benefiting single-crystal-based optics.

2. Diamond processing and fabrication of the kinoform lens

Several different approaches were made to etching diamond, two of which are presented here. They represent an attempt to balance three key issues in many plasma-etching processes: the etch rate, the r.m.s. surface roughness and the selectivity of diamond etch *versus* unintentional removal of a metal mask. Etching was performed with an Oxford Plasmalab 100 instrument, using an inductively coupled plasma and a cryogenically cooled wafer-holder as the temperature of the diamond during processing tends to increase well above the ambient temperature of the chamber. The diamond wafers used were 1 cm² and 120 μm-thick (supplied by Delaware Diamond Knives, <http://www.ddk.com/>). In the first process, illustrated schematically in Fig. 3(a), a mix of O₂ and Ar plasma was employed in three steps. In all three, the O₂ flow (5 × 10⁴ mm³ s⁻¹) was the same, and the difference between them lies in the argon flow; thus, the first step used 3 × 10³ mm³ s⁻¹ of argon, followed by the second step with 5 ×

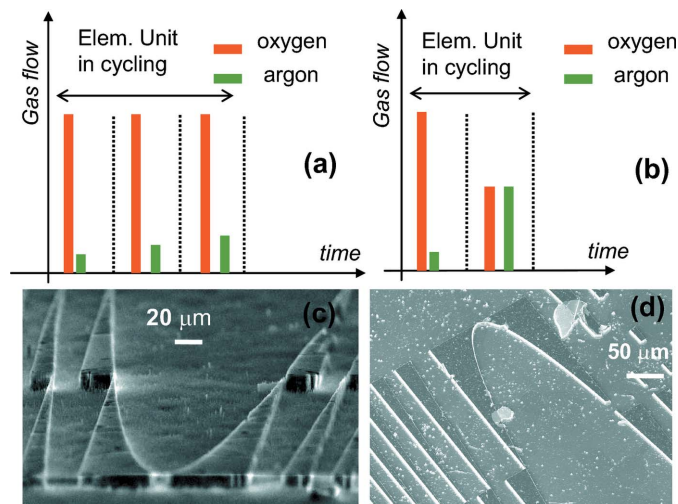


Figure 3
 (a) and (b) Two different approaches to cyclic etching of diamond: (a) the relative contribution of Ar to the total gas flow is small throughout the process, but steadily increases within each step in the cycle; (b) one of the two steps has equal flow of argon and oxygen. (c) and (d) Examples of close-up SEM images of two diamond lenses produced *via* (a) and (b), respectively.

10³ mm³ s⁻¹, and the final step with 8 × 10³ mm³ s⁻¹. This three-step sequence was repeated as many times as necessary, and is based on a similar approach we recently developed for ultradeep etching of silicon (Isakovic *et al.*, 2008). Others have had some success in etching diamond with a similar approach involving a gas mix based on O₂ (Ando *et al.*, 2002; Yamada *et al.*, 2006). The underlying idea behind using such a gas mixture is to combine physical factors that assist etching, like the kinetic energy of ions and the ion flux, with chemical etching processes. Because the surface roughness increases with increased argon flow, in the present experiments a small argon flow was used. Fig. 3(d) illustrates this point, *viz.* that a high contribution of Ar is not good for the surface quality; this figure illustrates the quality of an etched surface on small scale for the process where one of the two cycled steps uses 50% relative flow of Ar [etch process schematically depicted in Fig. 3(b)]. Although etching occurred, it is apparent that selectivity was poor, and portions of the patterned masked features of the kinoform lens were etched inadvertently. Table 1 gives further details of the etching parameters, and readers are reminded that their variations may be caused by changes in the carrier wafer, mask, aspect ratio and similar factors. In the present experiments, a bi-layer metal mask was used, where a layer of chromium (Cr) between 15 and 20 nm thick was deposited on diamond and then covered by a relatively thick layer of gold (Au), typically 150–200 nm. Undoubtedly, further efforts will go into developing a better mask to preclude problems similar to those encountered by other researchers etching diamond, most notably unintentional nanomasking (owing to sputtering of particles from the metal mask onto the surface of the diamond, where re-deposited metal particles act as nanomasks) (Ando *et al.*, 2002). The second process that might account for the slow etch

Table 1

Etching parameters for the two different diamond etching processes discussed.

Process I [Figs. 3(a) and 3(c)] uses cycling of steps A, B and C in that order. Process II [Figs. 3(b) and 3(d)] uses a combination of two pairs of steps: pair AC and pair AD that are cycled as a pair of steps for as long as needed (100–200 times typically).

Step	Q_{O_2} ($10^3 \text{ mm}^3 \text{ s}^{-1}$)	Q_{Ar} ($10^3 \text{ mm}^3 \text{ s}^{-1}$)	P_{ICP} (W)	P_{RF} (W)	P_{CHMBR} (Pa)	Time (s)	T (K)	Bias (V)	p_{He} (Pa)
A	50	3.0	800	15	1.6	30	253	0–20	667
B	50	5.0	800	15	2	30	253	0–40	667
C	50	8.0	900	15	2	30	253	0–40	667
D	20	20	900	20	2	20	253	0–45	667

rate stems from the possibility that diamond is transformed to other forms of carbon instead of being fully removed from the unmasked surface (Bello *et al.*, 2000). Fig. 3(c) shows an example of a hard X-ray kinoform refractive lens fabricated *via* the process from Fig. 3(a) where a moderate amount of Ar is used (3% to 8%), and which is used for the fabrication of the lens that led to results discussed in the rest of this report. While the faithful transfer of the numerically determined X-ray kinoform pattern is more readily visible in Fig. 3(c), this diamond nanofabrication approach is not without its problems. Some fine-scale surface inhomogeneity is still present, most likely a diamond equivalent of Si grass, that is likely to be removed in application of our processing on diamond of higher near-single-crystal quality.

Having determined the optimum process parameters, eight lenses were fabricated on a diamond wafer, four of which were for 11.3 keV ($f = 0.2$ m, lateral width of the lens 420 μm , numerical aperture 2.1×10^{-3} , etch depth 14 μm), and four were for 7.4 keV ($f = 0.2$ m, lateral width of the lens 460 μm , numerical aperture 2.3×10^{-3} , etch depth 12 μm); Fig. 4(b) shows one of the former, and Fig. 4(c) shows a central portion

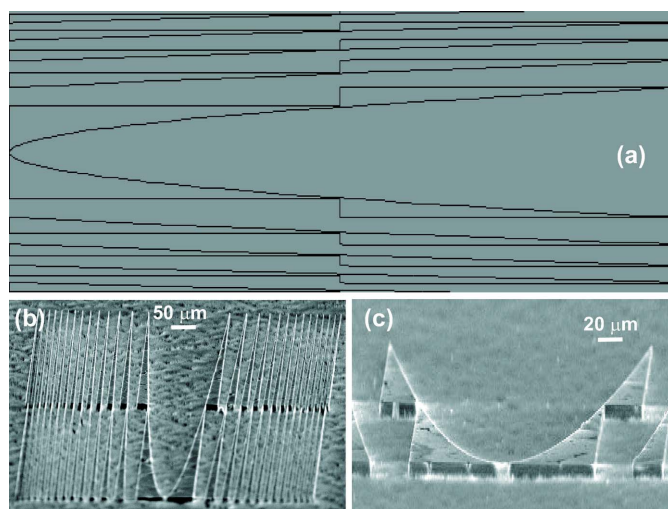
of one of the latter, while Fig. 4(a) displays a portion of the lithographic pattern, numerically determined as described in the *Introduction*. In panels (a) and (c) of Fig. 4, only the central portion of the lens is shown, for clarity, as the large number of half-shells tends to obscure the detailed structure of the lens. We used eight 2π phase shifts and two segments.

It is worth noting that the sidewalls are vertical, with no significant byproducts of etching, byproducts that may impede the performance of diamond kinoform refractive lens as a phase-preserving optics. After all the lithographic and etching steps, only three lenses were fully reproduced, indicating that the yield of the process is still lower than the yield for Si-based kinoform refractive lenses of similar design. However, using better quality diamond, improving the masking techniques and further tuning the steps of the plasma etch is expected to increase the success rate, and make this processing comparable with that of producing silicon kinoform lenses. Faithful transmission of the numerically designed kinoform pattern throughout the lithographic process was demonstrated; in particular, an etch lasting for 200 min gave an etch depth of 14 μm , leading to the average diamond etch rate of 70 nm min^{-1} .

Finally, in a separate experiment, two types of synthetic diamond were etched: the so-called ‘electronic’ grade (thermal conductivity $\lambda = 1800 \text{ W m}^{-1} \text{ K}^{-1}$) and the ‘optical’ grade ($\lambda = 1000 \text{ W m}^{-1} \text{ K}^{-1}$). As expected, the lower quality diamond (‘optical’ grade) showed more surface defects, pointing to the critical importance of having available a high-quality synthetic diamond to assure high-performance optics. Despite the sensitivity of the mode of nanofabrication to the type of diamond used, the focusing performance of both Si- and diamond-based kinoform refractive lenses demonstrably accommodated the presence of sub-20 nm-sized surface defects.

3. Measurements

To test its focusing performance, a diamond lens was installed directly into the hard X-ray beam at the Advanced Photon Source (APS) beamline 8-ID-I. Radiation from APS undulator A is delivered to the beamline *via* a windowless front-end. A highly polished horizontal-bounce Si mirror acts as a low-pass filter, reducing the power transmitted to the downstream monochromator that is comprised of a pair of water-cooled highly polished Ge(111) crystals. The X-ray beam


Figure 4

(a) Example of the central portion of the numerically designed kinoform lens, whose pattern is used for lithography. (b) The diamond kinoform lens ($E = 11.3$ keV, $f = 0.2$ m) used to obtain the focusing images. There is no mask owing to limitations in selectivity. (c) ‘Edge-on’ view of the central portion of a 7.4 keV lens from the perspective of the incoming X-rays, detailing a good verticality and relatively low ‘diamond grass’.

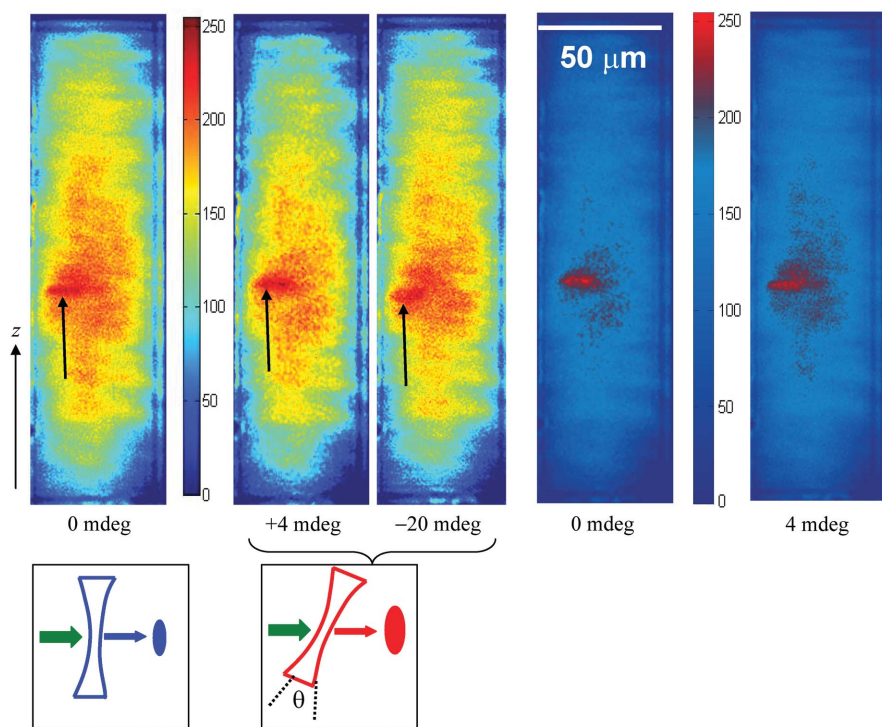


Figure 5 CCD images of the focal spot obtained after X-rays passed through the lens in Fig. 4, as registered by the YAG crystal/CCD system. Three images on the left for three different θ angle values are shown, out of more than 25 collected. Two false-color images are shown on the right for clarity (for 0 mdeg and 4 mdeg). The sketches show the definition of the angle θ . The elements of the drawings are not to scale. X-rays propagate into the page.

passes from a beampipe through a controllable slit opening onto the diamond kinoform lens with an energy of 11.3 keV, and a focal length $f = 0.2$ m. The typical opening of the slits early in the alignment is about $200 \times 500 \mu\text{m}$ ($H \times V$), and these numbers progressively decrease as the alignment of the lens is improved. X-rays pass through the single kinoform lens, are focused in one dimension, and hit a YAG (yttrium–aluminium–garnet) crystal. Fig. 5 shows microscope/CCD images of the focal spot. The Roper CoolSnap camera with $20\times$ objective was used for the final set of images, some of which are shown in Fig. 5. The smallest nominal pixel size of such a set-up is $0.32 \mu\text{m}$, but, in this initial report, determining the smallest focal spot size was not the goal, and other techniques, including knife-edge fluorescence, are more appropriate for such tasks. To test the focusing performance of the lens, its tilt was varied (expressed through the angle θ in Figs. 5 and 6) with respect to the direction of the propagating X-ray beam, to yield the changes in the size and shape of the focal spot depicted in Fig. 5. For clarity,

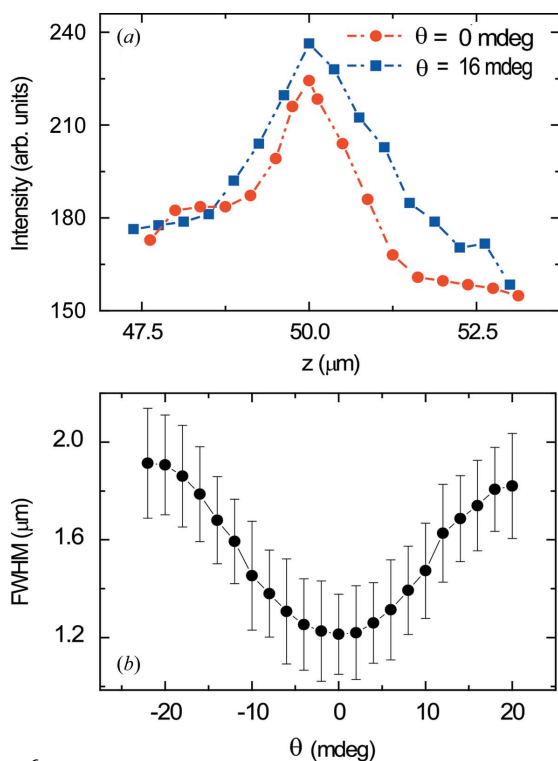


Figure 6 (a) Two intensity profiles across the focal spots from Fig. 5, for a pair of angular orientations of the diamond refractive lens. (b) FWHM (from peak fitting) for all the angular orientations of the lens tested.

a pair of false-color images is shown for two angular positions in the two right-most panels. The geometry of the experiment is illustrated in the sketches at the bottom of Fig. 5.

Although the high transmissivity of diamond is a powerful reason for using it as a material for X-ray lenses, one non-trivial difficulty was encountered during testing its focusing performance: a weak contrast. Namely, the lenses (with etch depths between 12 and $15 \mu\text{m}$) were fabricated out of self-supporting $120 \mu\text{m}$ -thick diamond wafers, so that the body of the plasma-etched lens and the remaining unetched substrate offered a weak contrast. Note that the depth of the etch in Fig. 4, approximately $14 \mu\text{m}$, generates a line-like image of the focal spot in the panels of Fig. 5, as would be expected for a one-dimensional planar kinoform lens. Ultimately, a tilt of about 50 mdeg sufficiently broadens the focal spot, so that the bright line near the center of the rectangles (in Fig. 5) almost completely disappears.

Images of the focal spot were sliced and their intensity plotted across the focal spot for a variety of θ angles (Fig. 6a). Fig. 6(b) plots the full width at half-maximum for all the angles. Two directions can be taken wherein such testing will afford further insights into the focusing performance of diamond kinoform refractive lenses: (i) refining the etch process should lead to a better quality and a larger depth of the diamond etch, and, (ii) improving the resolution of the detection of the focal spot (for example, *via* a standard knife-edge fluorescence test).

4. Conclusions

A reliable path is reported for designing and nanofabricating diamond kinoform refractive hard X-ray lenses. Comparisons of the material properties of silicon and diamond reveal different transmission efficiencies for the fixed energy range, with the overall advantage of diamond pointing towards future high-resolution X-ray focusing applications. A repeatable processing of diamond is discussed, offering clear possibilities for future improvements towards a more promising 150–200 nm min⁻¹ range for the etch rate, without a significant increase in surface roughness. Means of avoiding excessive damage to the diamond wafers, while producing near-vertical sidewalls and minimal ‘diamond grass’, are presented. The preliminary results of focusing tests show that a focal spot size of approximately 1 µm is achieved with a single $E = 11.3$ keV, $f = 0.2$ m, kinoform lens.

This manuscript has been authored by Brookhaven Science Associates, LLC under Contract No. DE-AC02-98CH10886 with the US Department of Energy. The United States Government retains, and the publisher, by accepting this article for publication, acknowledges, a world-wide license to publish or reproduce the published form of this manuscript, or allow others to do so, for United States Government purposes. We acknowledge supportive role of Chi-Chang Kao, J. Hill, D. Elliott and J. Smedley (all of BNL). AFI and KEL acknowledge support from BNL LDRD project 06-46 *Novel materials for hard X-rays optics*, and AFI thanks Professor P. G. Evans (University of Wisconsin) for stimulating discussions on X-ray optics and A. Woodhead and A. Acerbo (both of BNL) for technical assistance. Use of the Advanced Photon Source at Argonne National Laboratory was supported by the US Department of Energy, Office of Science, Office of Basic Energy Sciences, under Contract No. DE-AC02-06CH11357.

References

- Ando, Y., Nishibayashi, Y., Kobashi, K., Hirao, T. & Oura, K. (2002). *Diamond Relat. Mater.* **11**, 824–827.
- Aristov, V., Grigoriev, M., Kuznetsov, S., Shabelnikov, L., Yunkin, V., Weitkamp, T., Rau, C., Snigireva, I., Snigirev, A., Hoffmann, M. & Voges, E. (2000). *Appl. Phys. Lett.* **77**, 4058.
- Bello, I., Fung, M. K., Zhang, W. J., Lai, K. M., Wang, Y. M., Zhou, Z. F., Yu, R. K. W., Lee, C. S. & Lee, S. T. (2000). *Thin Solid Films*, **368**, 222–226.
- Bergemann, C., Keymeulen, H. & van der Veen, J. F. (2003). *Phys. Rev. Lett.* **91**, 204801.
- Bilderback, D. H., Hoffman, S. A. & Thiel, D. J. (1994). *Science*, **263**, 201–203.
- Chao, W., Harteneck, B., Liddle, J. A., Anderson, E. & Attwood, D. (2005). *Nature (London)*, **435**, 1210–1213.
- Cremer, J. T., Piestrup, M. A., Beguiristain, H. R., Gary, C. K., Pantell, R. H. & Tatchyn, R. (1999). *Rev. Sci. Instrum.* **70**, 3545.
- De Caro, L. & Jark, W. (2008). *J. Synchrotron Rad.* **15**, 176–184.
- Erko, A. I., Aristov, V. V. & Vidal, B. (1996). *Diffraction X-ray Optics*. Bristol: IOP Publishing.
- Evans-Lutterodt, K., Ablett, J. M., Stein, A., Tennant, D. M., Klemens, F. & Taylor, A. (2004). *Proc. SPIE*, **5539**, 73–79.
- Evans-Lutterodt, K., Stein, A., Ablett, J. M., Bozovic, N., Taylor, A. & Tennant, D. M. (2007). *Phys. Rev. Lett.* **99**, 134801.
- Goodman, J. W. (1996). *Introduction to Fourier Optics*. New York: McGraw-Hill.
- Hudson, J. A. (1984). *Appl. Opt.* **23**, 2292–2295.
- Isakovic, A. F., Evans-Lutterodt, K., Elliot, D., Stein, A. & Warren, J. B. (2008). *J. Vac. Sci. Technol.* **26**, 1182–1187.
- Jark, W., Matteucci, M. & Menk, R. H. (2008). *J. Synchrotron Rad.* **15**, 411–413.
- Jordan, J. A. Jr, Hirsch, P. M., Lesem, L. B. & Van Rooy, D. L. (1970). *Appl. Opt.* **9**, 1883–1887.
- Kang, H. C., Maser, J., Stephenson, G. B., Liu, C., Conley, R., Macrander, A. T. & Vogt, S. (2006). *Phys. Rev. Lett.* **96**, 127401.
- Lengeler, B., Tummler, J., Snigirev, A., Snigireva, I. & Raven, C. (1998). *J. Appl. Phys.* **84**, 5855.
- Mimura, H., Yumoto, H., Matsuyama, S., Sano, Y., Yamamura, K., Mori, Y. & Yabashi, M. (2007). *Appl. Phys. Lett.* **90**, 051903.
- Moreno, V., Roman, J. F. & Salgueiro, J. R. (1997). *Am. J. Phys.* **65**, 556–562.
- Nazmov, V., Shabel'nikov, L., Pantenburg, F.-J. Mohr, J., Reznikova, E., Snigirev, A., Snigireva, I., Kouznetsov, S. & DiMichiel, M. (2004). *Nucl. Instrum. Methods Phys. Res. B*, **217**, 409–416.
- Nöhammer, B., Hoszowska, J., Freund, A. K. & David, C. (2003). *J. Synchrotron Rad.* **10**, 168–171.
- Ognev, L. I. (2005). *Tech. Phys. Lett.* **31**, 314–315.
- Rau, C., Crecea, V., Peterson, K. M., Jemian, P. R., Richter, C.-P., Neuhausler, U., Schneider, G., Yu, X., Braun, P. V. & Robinson, I. K. (2006). *Proceedings of the 8th International Conference on X-ray Microscopy (XRM2005), IPAP Conference Series CS-7*, pp. 7–8.
- Schroer, C. G. (2006). *Phys. Rev. B*, **74**, 033405.
- Shastri, S. D., Almer, J., Ribbing, C. & Cederström, B. (2007). *J. Synchrotron Rad.* **14**, 204–211.
- Snigirev, A., Bjeoumikhov, A., Erko, A., Snigireva, I., Grigoriev, M., Yunkin, V., Erko, M. & Bjeoumikhova, S. (2007). *J. Synchrotron Rad.* **14**, 326–330.
- Suehiro, S., Miyaji, H. & Hayashi, H. (1991). *Nature (London)*, **352**, 385.
- Sweatt, W. C. (1977). *J. Opt. Soc. Am.* **67**, 803–808.
- Yamada, T., Yoshikawa, H., Uetsuka, H., Kumaragurubaran, S., Tokuda, N. & Shikata, S. (2006). *Diamond Relat. Mater.* **16**, 996–999.
- Yumoto, H., Mimura, H., Matsuyama, S., Handa, S., Sano, Y., Yabashi, M., Nishino, Y., Tamasaku, K. & Ishikawa, T. (2006). *Rev. Sci. Instrum.* **77**, 063712.